Check for updates

ChemistryEurope
Excellence in Chemistry Research Worldwide

Research Article
doi.org/10.1002/ceur.202500133

www.journal.chemistry-europe.org

Mechanistic Study of the Light-Initiated Generation of Free Diazoalkanes: Towards Photo-Orthogonal Synthesis

Ferdinand L. Pointner, Jonas Poll, Elina K. Taskinen, Vincent George, Tristan Ruff, Florian Rott, Gabriel Mayer, Niklas Gessner, Roger-Jan Kutta, Burkhard König, Patrick Nuernberger, Christian Ochsenfeld,* and Regina de Vivie-Riedle

In memory of Regina de Vivie-Riedle

An in-depth mechanistic study for the photogeneration of free diazoalkanes from *N*-tosylhydrazone precursors by combining observations from synthesis with spectroscopic and theoretical methods is presented. The *N*-tosylhydrazones have been previously established as donors for alkyl diazo species upon light irradiation, but exact mechanistic details of this photodissociation have remained elusive. Investigations of cyclohexane tosylhydrazone (CyNNTsH) by time-resolved FTIR spectroscopy proved the role of the deprotonated $CyNNTs^-$ as the light-harvesting species and revealed an intricate dependency of the thermal lifetime of the resulting diazoalkane on the deprotonating base. Computational studies including multiple approaches and levels of theory as well as rigorous benchmarking elucidated the dissociation mechanism via an allowed charge transfer state, a resulting destabilization of the dissociating bond, and a fast change of electronic character of the S_1. These insights allow to suggest specific reaction conditions for photolabile or previously incompatible reaction partners thus paving way towards photo-orthogonal synthetic strategies.

1. Introduction

Diazo compounds are highly versatile reagents in organic synthesis; they can be used both in ionic reactions (coupling with nucleophiles and electrophiles, 1,3-dipolar cycloadditions) or serve as radical acceptors and radical precursors themselves (**Scheme 1**A).[1] Moreover, further reaction modes can be easily unlocked by N_2 extrusion, giving rise to free singlet and triplet carbenes or metal carbenes as intermediates.[2–6] Importantly, though, not all reaction modes can be reached with every diazo compound and their reactivity is greatly directed by the electronic nature of their substituents and the environment. Thus, stabilized diazo compounds (acceptor–acceptor or donor–acceptor substituted) have been used to react with various coupling partners directly and have demonstrated broad potential for the formation of free and metal carbenes (Scheme 1B).[7,8] In contrast, the synthetic applications of nonstabilized diazo compounds (donor–donor) are less developed.[8,9]

Despite the high synthetic potential, the utilization of diazo compounds is still hampered by their toxicity and instability, leading to a considerable risk of explosion.[10] To avoid the direct handling of diazo compounds, stable precursors have been developed.[11] For example, access to diazo intermediates can be achieved via hydrazone oxidation (Ag_2O, MnO_2, $Cu(OAc)_2$, $Pb(OAc)_4$, and $PhI(OAc)_2$)[12–16] or via the thermal decomposition of deprotonated arylsulfonylhydrazone derivatives.[17] Although these strategies work well for the generation of stabilized diazo compounds,[17] the formation of aliphatic diazo compounds from arylsulfonylhydrazone derivatives requires temperatures exceeding 100 °C[18,19] or elaborate synthesis of 1,3,4-oxadiazolines.[20–22] As a result, the utilization of nonstabilized diazo compounds is limited by the harsh reaction conditions needed for their in situ synthesis. This limitation can be overcome by the photochemical conversion of the easily accessible and bench-stable *N*-tosylhydrazones into benzylic, aliphatic, and terminal diazo intermediates.[23] Using paraformaldehyde as a model electrophile, their synthetic potential in a formal C–H insertion reaction with carbonyl

F. L. Pointner, T. Ruff, F. Rott, C. Ochsenfeld, R. de Vivie-Riedle
Department Chemie
LMU Munich
Butenandtstraße 5–13, 81377 Munich, Germany
E-mail: christian.ochsenfeld@cup.uni-muenchen.de

J. Poll, G. Mayer, N. Gessner, R.-J. Kutta, P. Nuernberger
Institute for Physical and Theoretical Chemistry
Universität Regensburg
Universitätsstraße 31, 93053 Regensburg, Germany

E. K. Taskinen, V. George, B. König
Institute for Organic Chemistry
Universität Regensburg
Universitätsstraße 31, 93053 Regensburg, Germany

C. Ochsenfeld
Max-Planck-Institute for Solid State Research
Heisenbergstraße 1, 70569 Stuttgart, Germany

Supporting information for this article is available on the WWW under https://doi.org/10.1002/ceur.202500133

© 2025 The Author(s). ChemistryEurope published by Chemistry Europe and Wiley-VCH GmbH. This is an open access article under the terms of the Creative Commons Attribution License, which permits use, distribution and reproduction in any medium, provided the original work is properly cited.

© 2025 The Author(s). ChemistryEurope published by Chemistry Europe and Wiley-VCH GmbH

Research Article
doi.org/10.1002/ceur.202500133

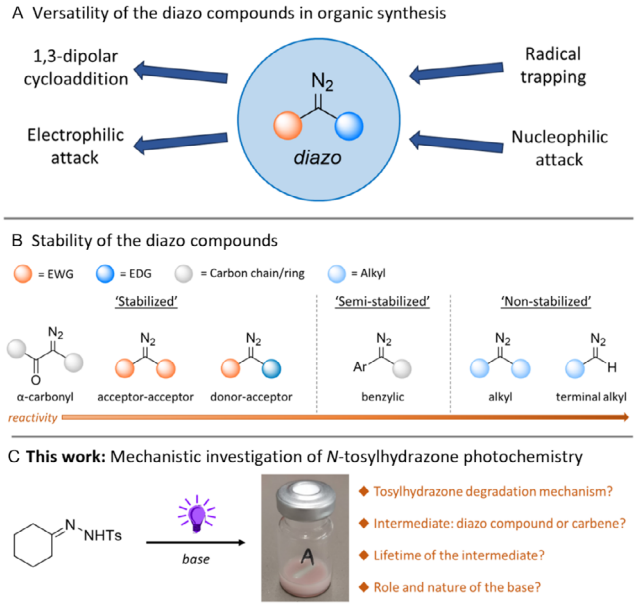

Scheme 1. A) Synthetic potential of the diazo compounds in organic chemistry. B) The effect of substituents, e.g., electron-withdrawing (EWG) and electron-donating groups (EDG), to the stability of the diazo compounds and their classifications. C) Experimental observation of the formation of colored solution upon irradiation of the *N*-tosylhydrazone precursor and the key mechanistic questions.

compounds (Büchner–Curtius–Schlotterbeck reaction) can be demonstrated. This method quickly gained recognition, and a variety of further applications, such as formal C–B insertion reactions[24–27] and [3 + 2] dipolar cycloadditions, emerged.[28–30] Under the used reaction conditions, the donor–donor diazo intermediates are remarkably stable, and the accumulation of a metastable diazo compound can be observed by a notable color formation often associated with diazo compounds.[7,21,31] Particularly, in the absence of a coupling partner (such as paraformaldehyde) or after complete conversion of it, the reaction mixture containing the photochemically generated diazo cyclohexane (CyN_2) retains its pink color for prolonged periods of time (Scheme 1C). Yet, the reasons for the accumulation under certain conditions and the underlying photochemical processes are not fully understood. However, the unexpected stability bears a potential, as the accumulation of these intermediates could open opportunities for pre-forming the donor–donor diazoalkanes prior to the addition of a coupling partner. This strategy would allow for the coupling of diazo intermediates with reaction partners that are photolabile or otherwise incompatible, e.g., with the deprotonated *N*-tosylhydrazones, hence providing the groundwork towards photo-orthogonal syntheses.

In our work, we combine computational and spectroscopic approaches, firstly to study the initial mechanism of the breaking of the covalent N—S bond. This includes identifying the photochemically active species and tracing the formation and stability of the products. Secondly, the excited-state processes are investigated elucidating critical factors in the dissociation process. Lastly, the importance of limiting the excess thermal energy in the synthesis of nonstabilized diazo compounds to increase their lifetime is discussed. The results of the study suggest potential opportunities to utilize the photo-initiated synthesis of diazo compounds in light-sensitive follow-up reactions, aiming towards light orthogonal synthetic pathways.

2. Results and Discussion

We chose the photodissociation of cyclohexane tosylhydrazone (CyNNTsH) as model reaction for the mechanistic investigations (**Scheme 2**). According to the previously proposed mechanism,[23] CyNNTsH is deprotonated by Cs_2CO_3 to the anionic species ($CyNNTs^-$) which after light absorption gives the photoexcited intermediate ($CyNNTs^{-*}$). This intermediate quickly dissociates into a tosylate anion (Ts^-) and the reactive diazocyclohexane (CyN_2).

First, the initial deprotonation of CyNNTsH to $CyNNTs^-$ is investigated. Upon deprotonation, the absorption of the first electronic transition undergoes a bathochromic shift from 284 nm for the original CyNNTsH to approximately 363 nm for its anionic form (**Figure 1**). Importantly, this redshift enables absorption at longer wavelengths allowing for selective irradiation of the deprotonated species.

The base-assisted photochemical cleavage of the *N*-tosylhydrazone CyNNTsH can be further monitored in the infrared (IR) spectral range (**Figure 2**). The initial protonated species CyNNTsH has a strong absorption signal at 1168 cm^{-1}, which then swiftly disappears upon addition of a base accompanied by the emergence of three new absorption bands (1224, 1123, and 1085 cm^{-1}) corresponding to the deprotonated species obtained with Cs_2CO_3 as the base (Figure 2A). The signal intensity is directly dependent on the concentration of the $CyNNTs^-$ anion and, consequently, proportional to the amount of base added until full deprotonation is reached. For example, in the case of 1,8-Diazabicyclo[5.4.0]undec-7-en (DBU), full deprotonation could be achieved after addition of 1.2 equivalents (120 mM), with any further addition of base having no significant effect on the observed signals. Other strong bases tested besides Cs_2CO_3 (DBU, KO*t*Bu, NaO*t*Bu, LiO*t*Bu) all resulted in disappearance of the signal at 1168 cm^{-1} indicating efficient deprotonation. However, small differences in the IR-spectra of the deprotonated species indicate subtle interactions with the corresponding counter ions. The importance of the initial deprotonation was further demonstrated by constant illumination of the sample, which resulted in clear decrease in the absorption signals assigned to $CyNNTs^-$ (Figure 2B) accompanied by a rise of a new absorption

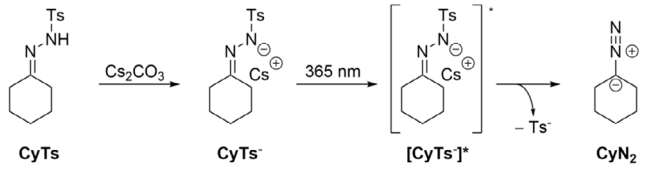

Scheme 2. Proposed mechanism for the photo-initiated decomposition of CyNNTsH to CyN_2 under basic conditions.

© 2025 The Author(s). ChemistryEurope published by Chemistry Europe and Wiley-VCH GmbH

27514765, 0, Downloaded from https://chemistry-europe.onlinelibrary.wiley.com/doi/10.1002/ceur.202500133 by Universitaet Regensburg, Wiley Online Library on [04/08/2025]. See the Terms and Conditions (https://onlinelibrary.wiley.com/terms-and-conditions) on Wiley Online Library for rules of use; OA articles are governed by the applicable Creative Commons License

Research Article
doi.org/10.1002/ceur.202500133

27514765, 0, Downloaded from https://chemistry-europe.onlinelibrary.wiley.com/doi/10.1002/ceur.202500133 by Universitaet Regensburg, Wiley Online Library on [04/08/2025]. See the Terms and Conditions (https://onlinelibrary.wiley.com/terms-and-conditions) on Wiley Online Library for rules of use; OA articles are governed by the applicable Creative Commons License

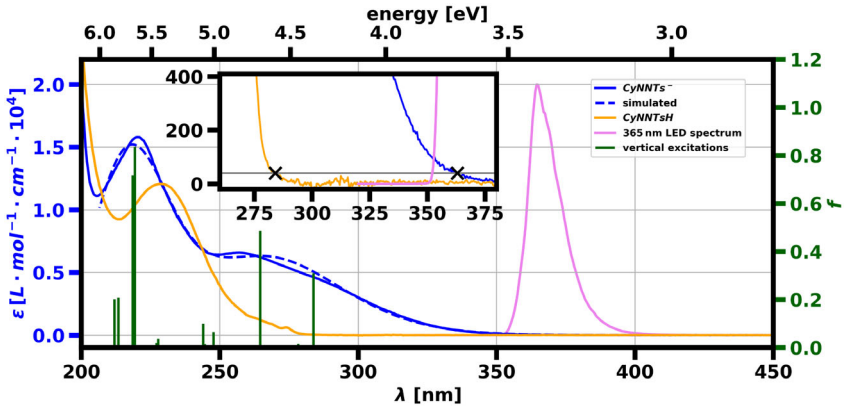

Figure 1. Absorption spectra of the pure CyNNTsH (orange) and CyNNTs$^-$, generated by deprotonation with DBU (solid blue) or simulated (dashed blue). The simulated spectrum was obtained by Gaussian broadening of the vertical excitations (green sticks) obtained from a TDA- ωB97X calculation. A correction was applied to the DBU spectrum to subtract the contribution of the base itself (see SI). The pink curve represents the emission of the LED used for excitation. The black crosses indicate where the extinction coefficients of absorption rises above 40 Lmol^{-1} cm^{-1}.

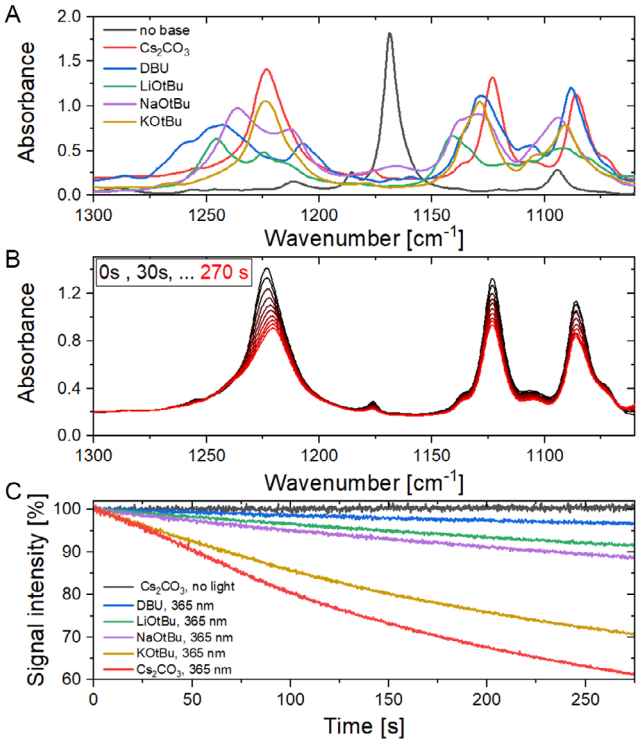

Figure 2. A) IR spectra of pure CyNNTsH (black) and its anionic form CyNNTs$^-$, formed from different bases. B) IR spectra of CyNNTs$^-$ in presence of Cs_2CO_3 under illumination at ca. 365 nm. C) Absorption changes in the range between 1275 and 1200 cm^{-1} assigned to CyNNTs$^-$ over time under different conditions as indicated.

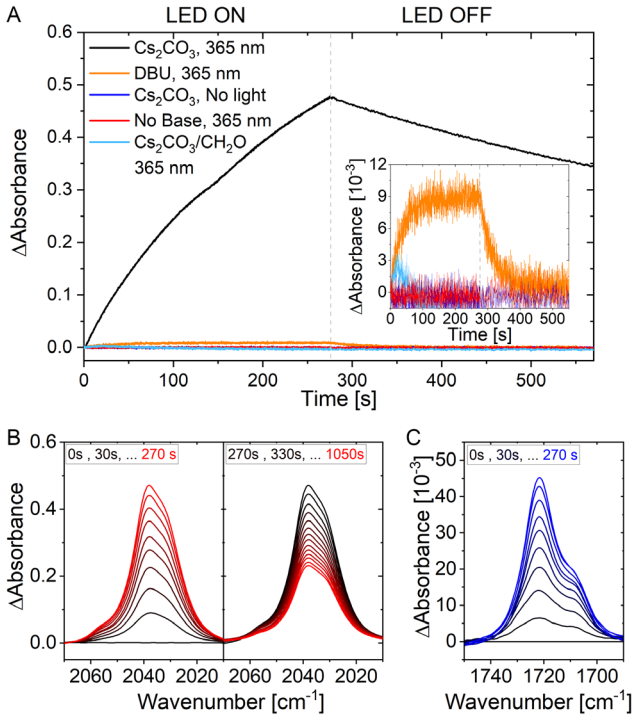

Figure 3. A) Difference absorption of the CyN_2 IR signal at 2038 cm^{-1} over time under different reaction conditions as indicated. The gray dashed line indicates the time range of illumination, if performed. A close up is given in the inset. B) The difference absorption spectra in the presence of Cs_2CO_3 at around 2038 cm^{-1} tracing CyN_2 formation upon illumination (left) and its decay in the dark afterwards (right). C) Arising absorption band of the product species during illumination of CyNNTsH in the presence of Cs_2CO_3 and paraformaldehyde.

band at 2038 cm^{-1} (**Figure 3**B). This band was assigned to a vibration of the diazo group from the resulting nonstabilized diazoalkane.[21,32] All the tested bases were capable of facilitating deprotonation, tosylate cleavage, and diazo compound formation upon illumination, albeit with a pronounced difference in the photolysis rate. Rates increase from DBU over LiO*t*Bu, NaO*t*Bu, KO*t*Bu, to Cs_2CO_3 (Figure 2C; see SI for detailed information). In contrast, without light or without the addition of a base, no decrease of the respective CyNNTs$^-$ or CyNNTsH signals nor formation of the diazo compound occurs, further supporting the necessity of base and light.[23,28]

Furthermore, the choice of base also influences the stability of the in situ generated diazo compounds. The free diazoalkane CyN_2, generated after the cleavage of the tosylate from the

© 2025 The Author(s). ChemistryEurope published by Chemistry Europe and Wiley-VCH GmbH

Research Article
doi.org/10.1002/ceur.202500133

27514765, 0, Downloaded from https://chemistry-europe.onlinelibrary.wiley.com/doi/10.1002/ceur.202500133 by Universitaet Regensburg, Wiley Online Library on [04/08/2025]. See the Terms and Conditions (https://onlinelibrary.wiley.com/terms-and-conditions) on Wiley Online Library for rules of use; OA articles are governed by the applicable Creative Commons License

CyNNTs$^-$, can be traced by its signal at 2038 cm^{-1}. In the presence of DBU, photochemical formation, starting from the deprotonated tosylhydrazone, and the thermal decomposition of the nonstabilized diazoalkane leads to a photostationary state of CyN_2 levels after around 100 s under the used continuous illumination conditions (Figure 3, orange-lined inset). In the presence of Cs_2CO_3 no photostationary state is achieved within 270 s of continuous illumination, which indicates either a photochemical pathway with a significantly higher reaction rate and/or an increased thermal stability of the photolysis product (Figure 3A). The thermal decomposition of the diazoalkane is manifested by an exponential decay of the absorption band at 2038 cm^{-1} in the dark and clearly dependent on the present base. While in the presence of DBU the decay of the diazoalkane has a time constant of ca. 28 s, it is significantly larger in presence of Cs_2CO_3 with ca. 17 min (see ESI for more detailed investigation).

The addition of the coupling partner paraformaldehyde traps the in situ generated diazoalkane.[23] The reaction prevents the accumulation of the free diazo compound, resulting in a quenching of the 2038 cm^{-1} signal accompanied by the formation of the aldehyde, identified by its C=O vibration at 1721 cm^{-1} (Figure 3C). This confirms a reaction pathway involving the diazoalkane instead of a carbene mediated pathway. As a result, the increased lifetime of the nonstabilized diazo compounds in presence of Cs_2CO_3 could be further utilized towards stepwise reactions where the diazo generation precedes the addition of a coupling partner. This, in turn, would allow coupling reactions with photosensitive substrates or with compounds which would react with the (deprotonated) *N*-tosylhydrazones in the ground state, thus paving way towards photo-orthogonal syntheses.

To obtain a better understanding on an atomistic level of the reaction mechanism, computational methods were used. First, the performances of different electronic structure methods were benchmarked against the experimental electronic absorption spectrum in the UV–vis spectral range. Here, DFT and linear response variants for excited states offer an established approach.[33,34] Due to commonly known downfalls of the theory, especially the accurate description of charge transfer (CT) states, rigorous benchmarking is necessary.[35] For such a benchmark, additional high level of theory methods, which are too expensive for production calculations, such as DFT-MRCI,[36] EOM-CCSD,[37] and XMS-CASPT2,[38] were used. The newly developed COOX method,[39] which is based on DFT including relaxed densities of excited states, allowed to confirm the presence of a low-lying CT state in the DFT framework. Seventeen functionals (for details see SI) were tested by comparing the optimally Gaussian-broadened and shifted computed spectrum to the experimental spectrum of the deprotonated CyNNTs$^-$ species. Single-point calculations were performed at the TDA-DFT/def2-TZVP/CPCM (acetonitrile)//r^{2}SCAN-3c/CPCM(acetonitrile) level of theory. Here, the ωB97X functional outperformed all other tested functionals with its visually almost perfect fit to the reference spectrum (Figure 1). Furthermore, all high level of theory methods agree on the lowest excited state with an allowed transition ($f > 0$) to be the CT state from the hydrazone to the tosyl moiety. Thus, the ωB97X functional was chosen for any further DFT-based calculations.

Preliminary gas-phase fewest switches surface hopping (FSSH) dynamics on the OM2-MRCI[40,41] level of theory gave a full dimensional bias-free overview of the reaction coordinates. The semiempirical OM2-MRCI method offers a computationally affordable approximation to a multireference solution and therefore is perfectly suited for exploratory access to even complex electronic structure problems, e.g., electronic states with multireference character, degeneration, and higher order excitation character.[40] Based on the simulations, the system can propagate along multiple reactive coordinates, namely the initial dissociating coordinate of the bond between the sulfur and adjacent nitrogen atom (R_{SN}), the carbon-nitrogen–nitrogen angle (A_{CNN}), and a secondary dissociation coordinate of the carbon–nitrogen bond (R_{CN}) (**Figure 4**A). Photolysis as indicated by an increase in R_{SN} takes place in the first 20 fs after excitation (Figure 4B), which is in agreement with the initially proposed mechanism. However, after the initial photolysis, the immediate thermolysis by elimination of dinitrogen and formation of the corresponding carbene, indicated by an increase in R_{CN}, occurs

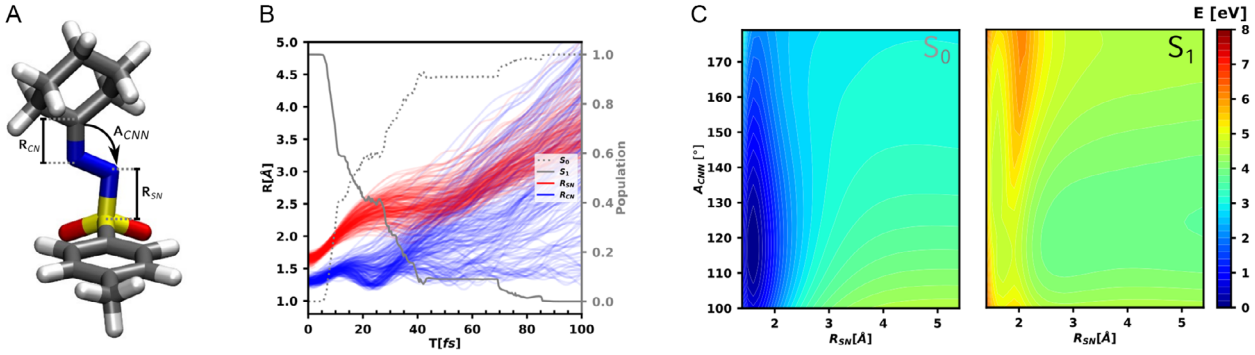

Figure 4. A) Three major critical coordinates of the CyNNTs$^-$ molecule that were investigated in detail: the bond stretch of the cyclohexyl carbon and the adjacent nitrogen (R_{CN}) and the angle between the aforementioned bond and the nitrogen–nitrogen bond (A_{CNN}), as well as the dissociation coordinate, namely the bond between the tosyl sulfur and the adjacent nitrogen (R_{SN}). B) Initial FSSH dynamics reveal the dissociation of the CyN_2 in the excited state, indicated by the increase in R_{SN}. A fast decay to the corresponding carbene, indicated by the increasing R_{CN}, is also observed. C) A 2D PES using the implicit solvation model and linear unrelaxed coordinates reveals a small barrier in the first excited singlet state S_1 along R_{SN}. Without further geometric relaxation the S_0 indicates a barrier free formation of the initial CyNNTs$^-$.

© 2025 The Author(s). ChemistryEurope published by Chemistry Europe and Wiley-VCH GmbH

Research Article
doi.org/10.1002/ceur.202500133

27514765, 0, Downloaded from https://chemistry-europe.onlinelibrary.wiley.com/doi/10.1002/ceur.202500133 by Universitaet Regensburg, Wiley Online Library on [04/08/2025]. See the Terms and Conditions (https://onlinelibrary.wiley.com/terms-and-conditions) on Wiley Online Library for rules of use; OA articles are governed by the applicable Creative Commons License

(Figure 4B). This ultrafast decay to the carbene is in contrast to the experiment. This discrepancy is most likely attributed to the lack of explicit solvation in the used model and the importance of a stabilizing solvent cage.[42] We also note that the dinitrogen release from diazo compounds often does not proceed efficiently from the lowest-lying excited singlet state but rather requires further excess energy, with isomerization to diazirine being a competitive pathway.[43–45] The importance of stabilization is furthermore emphasized by the unrelaxed TDA-ωB97X 2D potential energy surfaces (PES) in implicit solvation (Figure 4C). Here, the initial excitation from the ground state minimum into the S_1 leads to an almost barrier-free photolysis. Upon decay to the ground state, however, the minimum energy pathway leads back to the initial CyNNTs$^-$. Considering the Brownian motion, a solely impulse-controlled formation of free diazoalkane is highly unlikely. The results of an optimization of the dissociated product in implicit solvation accompanied by interpolated scans show a stabilization of the product species, albeit with unphysical aggregation of CyN_2 and Ts^- (see SI for details). These two computational approaches support the proposed reaction mechanism via the CT state of CyNNTs$^-$ and the formation of the free diazoalkane CyN_2 in the excited state, but either predict an unproductive or degrading decay in the ground state.

Next, the model was expanded by explicit solvation (for simulation details see SI) to understand the inhibition of direct thermolysis after the photogeneration of CyN_2. Due to the polar nature of the CyNNTs$^-$ and especially the CT state, the ONIOM method[46] using an subtractive electrostatic embedding scheme in conjunction with the GFN2-xTB method[47] was utilized offering a facile, more accurate, and computational efficient access to solute-solvent modeling compared to an unpolarizable QM/MM approach. The CyNNTs$^-$, CyNNTs^{-}* and the expected products CyN_2 and Ts^- were further optimized at the TDA-ωB97X/GFN2-xTB/MM level of theory including the solute (TDA-ωB97X) and solvent molecules (GFN2-xTB) in a range of 15 Å. Using in-house software to auto-generate large z-matrices of several hundreds of atoms with chemically relevant bonds, angles and dihedrals all atoms that were target of the optimization were included in a bi-linear interpolation of internal coordinates (see SI for movies of the corresponding coordinates q_1 and q_2). In these simulations, no aggregation of the product species but a stabilization in the solvent cage occurs. During dissociation, acetonitrile molecules are pushed away—which would correspond to a kinetic impedance in a dynamic picture—and other acetonitrile molecules move in the gap between CyN_2 and Ts^-.

Accordingly, the viscosity of the solvent can play a major role in the initial dissociation, as the solvent can dictate the inhibition of dissociation events.[42] This could partially explain previously performed reaction condition optimizations, where an inverse correlation between yield and solute viscosity could be observed (see SI for details). The excess charge of the now encapsulated Ts^- is furthermore effectively shielded by the solvent. A preassembly of cations to the CyNNTs$^-$ is expected to enhance this effect, by shielding the excess charge and preventing a recombination. Larger ions, like Cs^+, may shield the excess charge of the Ts^- species better than small ions, like Li^+. The solubility of DBU as organic base may inhibit the pre-assembly and thus the stabilizing effects. This is in line with the experimental data and highlights the potential of seemingly photophysically innocent parts of a reaction mixture in the optimization of reaction conditions. Previously, the presence of an electron-donor–acceptor (EDA) complex has been described to drive the conversion of benzylic *N*-tosylhydrazones using DBU as base.[29] This EDA complex is formed by bridging the aromatic moieties by two CH-π interactions. However, for aliphatic *N*-tosylhydrazones this binding mode and thus an EDA complex seems not feasible. An explicit solvation 2D PES from the linear interpolation of internal coordinates based on the TDA-ωB97X/GFN2-xTB/MM level (**Figure 5**A) shows similar features as the implicit one, as for example the small barrier in the Frank-Condon (FC) region of the S_1 along the dissociation coordinate and the energy degenerated seam at longer bond-lengths (CoIn seam) that facilitates fast nonradiative decay to the ground state. The now stabilized product minimum of the Ts^- and CyN_2 species is clearly visible. Due to the size of the system Hessians and thus Gibbs free energies could not be computed. Nevertheless, already enthalpies and estimated transition states provide a clear picture. The heterolytic ground state process, which is only slightly endergonic with a ΔH of 0.86 kcal mol^{-1}, is kinetically hampered with a barrier of 40.8 kcal mol^{-1} (transition state at $q_1 = -31.3$; $q_2 = -18.3$) (‡ Figure 5A S_0). In the excited state, however, the process

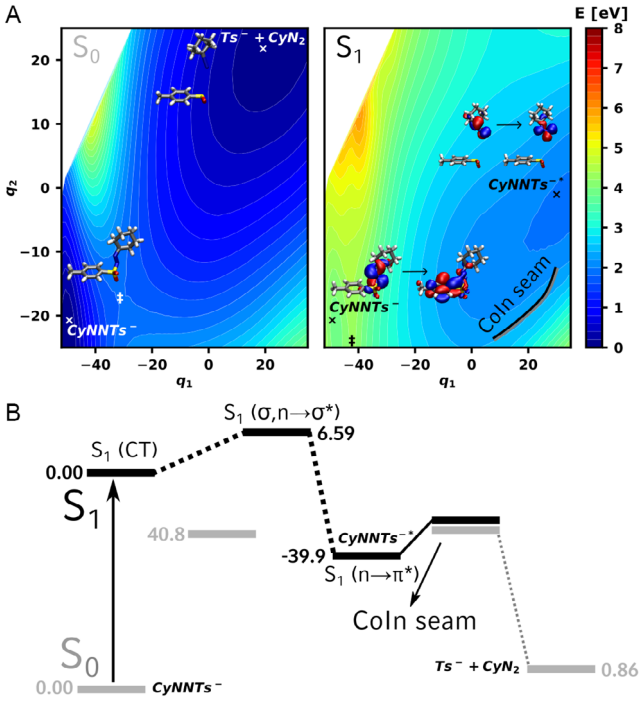

Figure 5. A) the 2D PES in the QM/QM/MM scheme elucidates the mechanism of the photogeneration of CyN_2. B) The initial CT state destabilizes R_{SN}—contained in q_1—which leads to a bond elongation across a small barrier. Here, the excited state quickly changes its character from CT to a $\sigma \rightarrow \sigma^*$ state and further to an $n \rightarrow \pi^*$ state. The relaxation to the ground state S_0 via an intersection seam of nearly degenerate energy leads to the solvent cage stabilized product CyN_2. Relative enthalpies adjacent to the critical points of the 2D PES are given in kcal mol^{-1} in gray for the S_0 and black for the S_1.

© 2025 The Author(s). ChemistryEurope published by Chemistry Europe and Wiley-VCH GmbH

Research Article
doi.org/10.1002/ceur.202500133

27514765, 0, Downloaded from https://chemistry-europe.onlinelibrary.wiley.com/doi/10.1002/ceur.202500133 by Universitaet Regensburg, Wiley Online Library on [04/08/2025]. See the Terms and Conditions (https://onlinelibrary.wiley.com/terms-and-conditions) on Wiley Online Library for rules of use; OA articles are governed by the applicable Creative Commons License

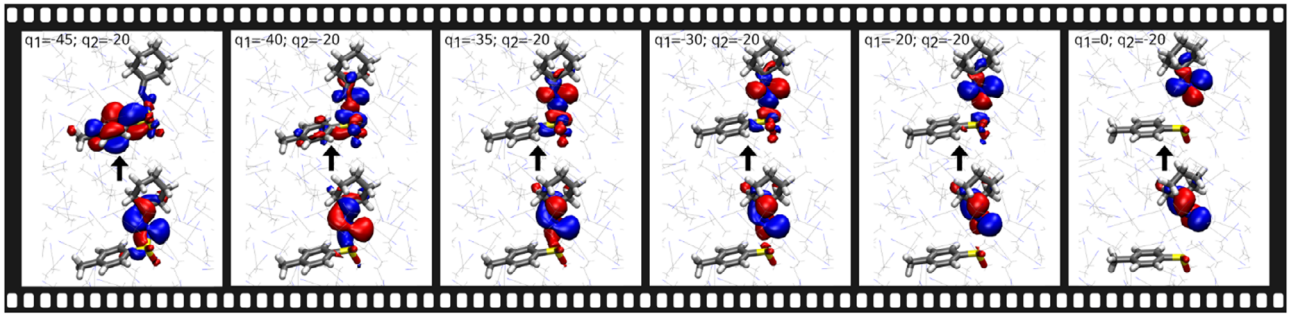

Figure 6. Visualization of the change of the excited state character along q_1 at $q_2 = -20$ using NTOs oft the first excited singlet state. Following the initial CT state from $q_1 = -45$, the character changes from a CT state to a σ, $n \rightarrow \sigma^*$ state at $q_1 = -40$ to finally a $n \rightarrow \pi^*$ state at $q_1 = 0$.

becomes homolytic and exergonic with a ΔH of -39.9 kcal mol^{-1} between CyNNTs$^-$ and CyNNTs^{-}*. Here, the barrier of 6.59 kcal mol^{-1} (transition state at $q_1 = -42.3$; $q_2 = -25.0$) (‡ Figure 5A S_1) is reduced by a factor of 5.65 compared to the barrier in the ground-state. The CoIn seam as well as the type of bond dissociation are corroborated by analysis on the CASSCF level of theory (for details see SI).

Therefore, the pathway via the excited state reduces the need of excess thermal energy, which in turn reduces the risk of unwanted follow up reactions, e.g., dinitrogen elimination. Here, the stabilization of the dissociated species furthermore plays a critical role, as the reassociation can either be prevented kinetically—risking instant carbene formation (see gas phase dynamics)—or by stabilizing the Ts$^-$ species by pre-assembly with suitable cations. Due to the complexity of excited-state processes, additionally, the character change of the excited state in an adiabatic picture may provide further insights (**Figure 6**). In the FC region, the S_1 can be characterized by a CT state from the hydrazone to the tosyl moiety. Since the dissociating σ-bond is conjugated with the lone pair of the nitrogen atoms, and the latter being the electron donor in the CT state, it is destabilized upon excitation. With increasing bond length (along q_1), the σ^*-orbital is lowered in energy, and the S_1 character changes to a σ, $n \rightarrow \sigma^*$ state. The mixing of σ^* and π^* orbitals is enhanced by an associated torsion of the hydrazone part, to the point where the S_1 can be characterized by an $n \rightarrow \pi^*$ excitation. This character can be associated to the product CyN_2 species.

The understanding of the excited-state processes provides an optimization opportunity of the productive reaction. As the photon energy in the nonradiative decay process leads to excess energy in the ground state, that can lead to the carbene species, the lowest possible photon energy to initiate the dissociation process is desirable. Further, due to the CT nature of the excited state and the tosyl moiety being the electron acceptor, electron poorer sulfonic acid derivatives may result in a bathochromic shift of the first electronic transition.

3. Conclusion

By combining synthetic, spectroscopic, and computational methods, the mechanism of the previously reported photolysis of cyclohexyl tosylhydrazone (CyNNTsH) towards its diazo analog has been elucidated. Using UV-Vis and IR spectroscopy, the deprotonated CyNNTs$^-$ anion was identified as the reactive intermediate in the formation of the diazo compound, and the necessity of both a base and light for tosylate cleavage was confirmed. The presence of the diazo compound was verified by the characteristic absorption band at 2038 cm^{-1}. The stability of the diazo compounds was shown to be influenced by the photolysis reaction conditions. In the presence of Cs_2CO_3 as deprotonating base, the lifetime of diazo cyclohexane is ca. 17 min, representing a 30-fold increase compared to 28 s in the case of DBU. Quantum mechanically determined 2D-PES revealed an interplay between the lone-pair σ-bond hyperconjugation and the CT state, steering the dissociation of the N—S bond. It further turned out that the stabilizing effects of the solvent cage is critical for stable product formation. An accumulation of the nonstabilized diazo compound was achieved in this excited state process using Cs_2CO_3 as base. By decreasing excess thermal energy and the stabilization of the product species, unproductive and decaying pathways could be minimized. This represents the prospects for photo-orthogonal synthesis by increasing the concentration in the photostationary state and the lifetime of nonstabilized diazo compounds for stepwise reactions. This contrasts with the previously needed continued irradiation and hopefully encourages the harnessing of new synthetic opportunities. Simultaneously, the base DBU can be a suitable alternative in a one-pot reaction, where continued illumination does not interfere in the follow-up reaction with the diazo compound.

Acknowledgements

This work was supported by the Deutsche Forschungsgemeinschaft [DFG (German Science Foundation) grants TRR 325–444632635 and GRK 2620–426795949]. C.O. acknowledges additional financial support as Max-Planck-Fellow at the Max Planck Institute for Solid State Research (MPI-FKF) Stuttgart.

Conflict of Interest

The authors declare no conflict of interest.

© 2025 The Author(s). ChemistryEurope published by Chemistry Europe and Wiley-VCH GmbH

Research Article
doi.org/10.1002/ceur.202500133

27514765, 0, Downloaded from https://chemistry-europe.onlinelibrary.wiley.com/doi/10.1002/ceur.202500133 by Universitaet Regensburg, Wiley Online Library on [04/08/2025]. See the Terms and Conditions (https://onlinelibrary.wiley.com/terms-and-conditions) on Wiley Online Library for rules of use; OA articles are governed by the applicable Creative Commons License

Data Availability Statement

The data that support the findings of this study are available in the supplementary material of this article.

Keywords: diazo compounds · photochemistry · reaction mechanisms

[1] J. Wang, *Tetrahedron Lett.* **2022**, *108*, 154135.
[2] G. Burdzinski, M. S. Platz, *J. Phys. Org. Chem.* **2010**, *23*, 308.
[3] D. Kvaskoff, H. Lüerssen, P. Bednarek, C. Wentrup, *J. Am. Chem. Soc.* **2014**, *136*, 15203.
[4] P. Costa, W. Sander, *Angew. Chem. Int. Ed.* **2014**, *53*, 5122.
[5] J. Knorr, P. Sokkar, S. Schott, P. Costa, W. Thiel, W. Sander, E. Sanchez-Garcia, P. Nuernberger, *Nat. Commun.* **2016**, *7*, 12968.
[6] V. Brusar, M. Forjan, I. Ljubić, M. Alešković, K. Becker, S. Vdović, *J. Org. Chem.* **2023**, *88*, 4286.
[7] Z. Zhang, V. Gevorgyan, *Chem. Rev.* **2024**, *124*, 7214.
[8] Z. Yang, M. L. Stivanin, I. D. Jurberg, R. M. Koenigs, *Chem. Soc. Rev.* **2020**, *49*, 6833.
[9] P. Yamini, M. Junaid, D. Yadagiri, *Chem.—An Asian J* **2025**, *20*, e202401239.
[10] S. P. Green, K. M. Wheelhouse, A. D. Payne, J. P. Hallett, P. W. Miller, J. A. Bull, *Org. Process Res. Dev.* **2020**, *24*, 67.
[11] M. Liu, C. Uyeda, *Angew. Chem. Int. Ed.* **2024**, *63*, e202406218.
[12] I. Bhatnagar, M. V. George, *J. Org. Chem.* **1967**, *32*, 2252.
[13] A. J. Clark, W. F. Pickering, *J. Inorg. Nuc. Chem.* **1967**, *29*, 836.
[14] B. Wei, T. A. Hatridge, C. W. Jones, H. M. L. Davies, *Org. Lett.* **2021**, *23*, 5363.
[15] D. H. R. Barton, J. C. Jaszberenyi, W. Liu, T. Shinada, *Tetrahedron* **1996**, *52*, 14673.
[16] T. L. Holton, H. Schechter, *J. Org. Chem.* **1995**, *60*, 4725.
[17] J. R. Fulton, V. K. Aggarwal, J. de Vicente, *Eur. J. Org. Chem.* **2005**, *2005*, 1479.
[18] R. A. Henry, D. W. Moore, *J. Org. Chem.* **1967**, *32*, 4145.
[19] Z. Liu, P. Sivaguru, G. Zanoni, X. Bi, *Acc. Chem. Res.* **2022**, *55*, 1763.
[20] P. Dingwall, A. Greb, L. N. S. Crespin, R. Labes, B. Musio, J.-S. Poh, P. Pasau, D. C. Blakemore, S. V. Ley, *Chem. Commun.* **2018**, *54*, 11685.
[21] A. Greb, J.-S. Poh, S. Greed, C. Battilocchio, P. Pasau, D. C. Blakemore, S. V. Ley, *Angew. Chem. Int. Ed.* **2017**, *56*, 16602.
[22] K. Orłowska, J. V. Santiago, P. Krajewski, K. Kisiel, I. Deperasińska, K. Zawada, W. Chaładaj, D. Gryko, *ACS Catal.* **2023**, *13*, 1964.
[23] H. Wang, S. Wang, V. George, G. Llorente, B. König, *Angew. Chem. Int. Ed.* **2022**, *61*, e202211578.
[24] A. Valdés-Maqueda, M. Plaza, C. Valdes, *Chem. Sci.* **2024**, *15*, 19633.
[25] P.-K. Peng, C. P. Donald, Z. Dong, J. A. May, *Org. Lett.* **2024**, *26*, 3397.
[26] M. Junaid, S. Happy, D. Yadagiri, *Chem. Commun.* **2024**, *60*, 2796.
[27] Á. Valdés-Maqueda, L. López, M. Plaza, C. Valdés, *Chem. Sci.* **2023**, *14*, 13765.
[28] V. George, B. König, *Chem. Commun.* **2023**, *59*, 11835.
[29] Y. Zhang, Y. Li, S.-F. Ni, J.-P. Li, D. Xia, X. Han, J. Lin, J. Wang, S. Das, W.-D. Zhang, *Chem. Sci.* **2023**, *14*, 10411.
[30] A. I. Alfano, M. Smyth, S. Wharry, T. S. Moody, M. Nuño, C. Butters, M. Baumann, *Chem. Commun.* **2024**, *60*, 7037.
[31] A. J. Wommack, J. S. Kingsbury, *J. Org. Chem.* **2013**, *78*, 10573.
[32] P. Yates, B. L. Shapiro, N. Yoda, J. Fugger, *J. Am. Chem. Soc.* **1957**, *79*, 5756.
[33] W. Kohn, L. J. Sham, *Phys. Rev.* **1965**, *140*, A1133.
[34] S. Hirata, M. Head-Gordon, *Chem. Phys. Lett.* **1999**, *314*, 291.
[35] F. L. Kiss, B. P. Corbet, N. A. Simeth, B. L. Feringa, S. Crespi, *Photochem. Photobiol. Sci.* **2021**, *20*, 927.
[36] C. M. Marian, A. Heil, M. Kleinschmidt, *WIREs Comput. Mol. Sci.* **2019**, *9*, e1394.
[37] J. F. Stanton, R. J. Bartlett, *J. Chem. Phys.* **1993**, *98*, 7029.
[38] T. Shiozaki, W. Győrffy, P. Celani, H.-J. Werner, *J. Chem. Phys.* **2011**, *135*, 081106.
[39] J. Kussmann, Y. Lemke, A. Weinbrenner, C. Ochsenfeld, *J. Chem. Theory Comput.* **2024**, *20*, 8461.
[40] P. O. Dral, X. Wu, L. Spörkel, A. Koslowski, W. Weber, R. Steiger, M. Scholten, W. Thiel, *J. Chem. Theory Comput.* **2016**, *12*, 1082.
[41] E. Fabiano, T. W. Keal, W. Thiel, *Chem. Phys.* **2008**, *349*, 334.
[42] M. T. Peschel, J. Kussmann, C. Ochsenfeld, R. de Vivie-Riedle, *Phys. Chem. Chem. Phys.* **2024**, *26*, 23256.
[43] S. M. Korneev, *European J. Org. Chem.* **2011**, *2011*, 6153.
[44] P. Rudolf, J. Buback, J. Aulbach, P. Nuernberger, T. Brixner, *J. Am. Chem. Soc.* **2010**, *132*, 15213.
[45] A. Bogdanova, V. V. Popik, *J. Am. Chem. Soc.* **2003**, *125*, 1456.
[46] M. Svensson, S. Humbel, R. D. J. Froese, T. Matsubara, S. Sieber, K. Morokuma, *J. Phys. Chem.* **1996**, *100*, 19357.
[47] C. Bannwarth, S. Ehlert, S. Grimme, *J. Chem. Theory Comput.* **2019**, *15*, 1652.

Manuscript received: April 28, 2025
Revised manuscript received: July 1, 2025
Version of record online:

© 2025 The Author(s). ChemistryEurope published by Chemistry Europe and Wiley-VCH GmbH